



INSTITUT DE FRANCE
Académie des sciences

Comptes Rendus

Chimie

Mihaela Muresanu, Andreea Eliescu, Eugenia-Corina Ignat,
Gabriela Carja and Nicoleta Cioatera

Different routes of MgAl-LDH synthesis for tailoring the adsorption of Pb(II) pollutant from water


Volume 25, Special Issue S3 (2022), p. 281-292

Published online: 30 May 2022

<https://doi.org/10.5802/crchim.184>

Part of Special Issue: Active site engineering in nanostructured materials for energy, health and environment

Guest editors: Ioana Fechete (Université de Troyes, France) and Doina Lutic (Al. I. Cuza University of Iasi, Romania)

 This article is licensed under the
CREATIVE COMMONS ATTRIBUTION 4.0 INTERNATIONAL LICENSE.
<http://creativecommons.org/licenses/by/4.0/>



Les Comptes Rendus. Chimie sont membres du
Centre Mersenne pour l'édition scientifique ouverte
www.centre-mersenne.org
e-ISSN : 1878-1543



Active site engineering in nanostructured materials for energy, health and environment /
*Ingénierie de sites actifs dans les matériaux nanostructurés pour l'énergie, la santé et
l'environnement*

Different routes of MgAl-LDH synthesis for tailoring the adsorption of Pb(II) pollutant from water

Mihaela Mureseanu^{Ⓢ a}, Andreea Eliescu^a, Eugenia-Corina Ignat^b, Gabriela Carja^{Ⓢ*, b}
and Nicoleta Cioatera^{Ⓢ*, a}

^a University of Craiova, Faculty of Sciences, Department of Chemistry, Calea
Bucuresti, 1071, Craiova, Romania

^b Faculty of Chemical Engineering and Environmental Protection, Technical
University of Iasi, 71 D. Mangeron, Iasi, Romania

E-mails: mmureseanu32@gmail.com (M. Mureseanu), andreea200752@yahoo.com
(A. Eliescu), eugenia-corina.ignat@student.tuiasi.ro (E.-C. Ignat), carja@uaic.ro
(G. Carja), nicoletacioatera@yahoo.com (N. Cioatera)

Abstract. In this study, new adsorbents based on MgAl-LDHs were synthesized using combined precipitation (co-precipitation) route by modifying temperature and ageing time synthesis parameters, thus tailoring the adsorption capacity of Pb(II) ions from water. The synthesized materials were characterized by SEM, FTIR, XRD and N₂ adsorption-desorption techniques, highlighting the specific lamellar structure of layered double hydroxides (LDHs), as well as the functional groups present on the adsorbent's surface. The maximum adsorption capacity for Pb(II) ions was 1151.97 mg/g for the MgAl-LDH synthesized at 55 °C and aged for 24 h. Sorption of Pb(II) ions occurs not only through co-precipitation in the form of characteristic compounds, Pb(OH)₂, PbCO₃ or Pb₃(CO₃)₂(OH)₂, but also by complexation with surface hydroxyl groups.

Résumé. Dans cette étude, de nouveaux adsorbants à base de MgAl-LDH ont été synthétisés par voie de co-précipitation en modifiant comme paramètres de synthèse la température et le temps de maturation et utilisés pour contrôler la capacité d'adsorption des ions Pb(II) de l'eau. Les matériaux synthétisés ont été caractérisés par des techniques d'adsorption-désorption de N₂, SEM, FTIR, XRD, qu'il a mis en évidence la structure lamellaire spécifique des LDH, ainsi que les groupements fonctionnels présents à la surface de l'adsorbant. La capacité maximale d'adsorption des ions Pb(II) était de 1151,97 mg/g pour le MgAl-LDH synthétisé à 55 °C et vieilli pendant 24 h. La sorption des ions Pb(II) se fait par précipitation (co-précipitation) sous forme de composés caractéristiques, Pb(OH)₂, PbCO₃ ou Pb₃(CO₃)₂(OH)₂, mais aussi le mécanisme de complexation avec des groupements hydroxyles de surface doit être pris en compte.

Keywords. LDH, Co-precipitation, Crystallinity, Pb(II) adsorption, Heavy metals, Adsorption capacity.

Mots-clés. LDH, Co-précipitation, Cristallinité, Adsorption de Pb(II), Métaux lourds, Capacité d'adsorption.

Published online: 30 May 2022

* Corresponding authors.

1. Introduction

Contamination of wastewater due to industrial spills creates an alarming situation, with the presence of numerous pollutants in drinking water leading to undesirable effects on ecosystems and human life [1]. These non-degradable wastes, including heavy metals or toxic organic compounds, result from different industries (fertilizers, metallurgy, leather, mining, galvanizing, pesticides, electrolysis, electro-osmosis, plastics, batteries) and end up in the water directly or indirectly. The effect of these compounds can be toxic, mutagenic, neurotoxic or carcinogenic [2,3]. The most common heavy metal ions in polluted waters are: Pb(II), Hg(II), Cr(III), Cd(II), Cu(II), Ni(II) and As(III) [4]. According to the World Health Organization [5], the presence of lead in concentrations exceeding the allowed limit (>0.1 mg/L) can affect the nervous system, kidneys, brain, liver and can lead to health problems such as hepatitis, nephritic syndrome, anemia, and so on [6]. Because it has affinity for the thiol (-SH), phosphate (PO_4^{3-}) and oxo (=O) groups, which are found in the structure of enzymes, ligands or biomolecules in the human body, lead can affect the living organism's membrane permeability and hemoglobin synthesis [7]. Therefore, efforts have been devoted to develop efficient methods for its removal. Conventional methods for removing pollutants include precipitation, reduction, adsorption, coagulation, membrane filtration [4], but these have disadvantages such as the use of non-renewable materials, high cost and the generation of toxic products.

Various studies have shown that hydrotalcites, including anionic clays and layered double hydroxides (LDHs) are effective materials for adsorption/removal of heavy metals from aqueous solutions [8,9]. These are a class of two-dimensional nanostructured compounds, characterized by a stratified lamellar structure similar to brucite [$\text{Mg}(\text{OH})_2$] [10]. LDHs are represented by the general formula $[\text{M}_{1-x}^{\text{II}}\text{M}_x^{\text{III}}(\text{OH})_2]^{x+}(\text{A}_{x/n}^{n-}) \cdot m\text{H}_2\text{O}$, where M^{2+} and M^{3+} are the divalent and trivalent metal cations, respectively, A^{n-} are the positive charge-compensating anions, located in the interlamellar space; x is the stoichiometric coefficient defined as the ratio of $\text{M}^{3+}/(\text{M}^{2+} + \text{M}^{3+})$ [11], whose values are typically in the 0.25–0.33 range [12]. The LDH layers overlap and form hydrogen bonds. Some of the interlamellar

anions can be replaced with other ions when the LDHs are immersed in their aqueous solution. Also, the metal cations from the hydroxide layers can be replaced by other metal cations with similar ionic radius through the isomorphic substitution process during the synthesis of the LDHs. Thus, materials with controllable components for specific applications can be obtained [13]. LDHs possess unique properties, such as large surface areas, high ion exchange capacity, are versatile and economical materials, with various applications in many fields such as: catalysis [14,15] pharmaceutical's transport systems [16,17], additives for polymers [18], adsorption [19].

$\text{Mg}_2\text{Al-LDH}$ hydrotalcite was investigated in Pb(II) adsorption process, exhibiting an adsorption capacity of 66.16 mg/g [19]. By substituting Al ions with Fe ions, a much higher capacity (865.36 mg/g) was obtained [20]. The FeMnMg-LDH-type material, obtained by the combined precipitation (co-precipitation) method, was used to remove Pb(II) ions from wastewater, having an adsorption capacity of 421.42 mg/g [13]. MgAl-LDH-type materials intercalated with different amino acids (phenylalanine, tyrosine, serine) showed good adsorption capacity for Pb(II) ions. The highest capacity was obtained for the MgAl-phenylalanine-LDH material (852 mg/g) [21]. Inspired by mussel adhesion protein, Yang *et al.* [22] have synthesized MgAl-LDH/carbon fiber film modified by polydopamine for highly efficient removal of Pb^{2+} (1223.15 mg/g).

The aim of this study was to characterize and determine the maximum sorption capacity of Pb(II) ions for six adsorbents based on MgAl-LDHs, synthesized using co-precipitation route by modifying some of the synthesis parameters (temperature, ageing time) in order to tailor their adsorption properties.

2. Materials and methods

2.1. Reagents and materials

All experiments were performed using analytical grade reagents, without prior purification. $\text{Al}(\text{NO}_3)_3 \cdot 9\text{H}_2\text{O}$, $\text{Mg}(\text{NO}_3)_2 \cdot 6\text{H}_2\text{O}$, Na_2CO_3 , NaOH (Aldrich, 99.9%), were used for the LDHs synthesis. The sorption experiments were performed using a $1500 \text{ mg} \cdot \text{L}^{-1}$ Pb(II) stock solution, prepared by dissolving 2.385 g $\text{Pb}(\text{NO}_3)_2$ in 1000 mL of distilled

water. The working solutions with different Pb(II) concentrations were prepared by its dilution. For Flame Atomic Absorption Spectrometry (FAAS) measurements, the calibration curve was recorded in the concentration range 1–20 mg·L⁻¹ using a standard Pb(II) solution of 1000 mg·L⁻¹. The pH was adjusted in the range 2–6 using 0.1 M HCl or 0.1 M NaOH solutions.

2.2. LDHs synthesis

All the LDHs were prepared by a co-precipitation method similar to that described in [23]. Briefly, MgAl-LDH containing Mg²⁺ and Al³⁺ (Mg²⁺/Al³⁺ = 2/1) as cations in the LDHs layers was prepared by the slow addition of a 1 M aqueous solution of Mg(NO₃)₂·6H₂O and Al(NO₃)₃·9H₂O, to a Na₂CO₃ (0.5 × 10⁻² M) solution under stirring. The synthesis temperatures and the ageing time of the samples were optimized as controlled variable synthesis parameters. The obtained MgAl-LDH is symbolized as P^Y(X), where X represents the synthesis temperature (X is equal to 5 °C, 15 °C, 30 °C and 55 °C) and Y is the ageing time of the obtained sample (Y = 24 h or 1 h). For all the samples the pH value was kept constant at 9, by adding suitable quantities of 0.1 M NaOH aqueous solution. The obtained precipitates were recovered by filtration, washed several times with distilled water to remove soluble salts and dried at 80 °C under vacuum overnight. Following these procedures, the synthesized MgAl-LDHs were further denoted as P²⁴(5), P²⁴(15), P²⁴(30), P¹(30), P²⁴(55) and P¹(55).

2.3. Characterization techniques

Scanning electron microscopy (SEM) analyses were performed at 2 kV using a Hitachi SU8010 microscope. The elemental composition was determined by energy dispersive X-ray spectroscopy (EDX) at an acceleration voltage of 15 kV. A Bruker Alpha spectrometer with ZnSe crystal and an attenuated total reflectance (ATR) module was used for the Fourier transform infrared spectroscopy (FTIR) analyses, the spectra being recorded in the spectral range 4000–400 cm⁻¹, at a resolution of 4 cm⁻¹.

X-ray diffraction (XRD) spectra were recorded using an X-ray diffractometer at 2θ = 5–80°. XRD spectra were recorded using a Rigaku SmartLab X-ray

diffractometer with a CuKα radiation (λ = 1.5406 Å) in 2θ range 5–80°. The crystallite sizes of the investigated samples were calculated from XRD data using Scherrer equation:

$$D = \frac{0.9 \cdot \lambda}{\beta \cdot \cos \theta},$$

where *D* is the crystallite size (nm), λ is the wavelength of CuKα radiation (0.15404 nm), and β is the full width at half maximum (FWHM) in radians for the (003) reflection.

The *a* and *c* lattice parameters of the LDH hexagonal crystalline structure were calculated using *d*₍₁₁₀₎ and *d*₍₀₀₃₎ lattice spacing, respectively:

$$\frac{1}{d^2} = \frac{4}{3} \frac{h^2 + hk + k^2}{a^2} + \frac{l^2}{c^2},$$

where *h*, *k*, *l* are the Miller indices of the reflection planes.

The specific surface area and porosity parameters were determined by a N₂ adsorption-desorption technique at -196 °C with an Automated Gas Sorption Data Quantochrome Instrument. Specific surface area was calculated based on Brunauer-Emmet-Teller (BET) isotherm model, the pore volume was determined from isotherm at the end of capillary condensation and the pore size distribution from the desorption branch using Barret-Joyner-Halenda (BJH) method and Harkins-Jura standard isotherm. The pH measurement was performed with a pH meter (WTW Multi 9430-Inolab) equipped with a pH Sentix 98 sensor (±0.04 precision) with temperature compensation. The concentration of lead was determined by FAAS with a GBS Avanta spectrometer with air-acetylene flame and background correction with deuterium lamp. The concentration of Mg²⁺ was examined using inductively coupled plasma optical emission spectrometry (ICP-OES Avio 500 Perkin Elmer).

2.4. Sorption experiments of Pb(II) ions

The study of the sorption capacity of Pb(II) ions from aqueous solutions on P²⁴(5), P²⁴(15), P²⁴(30), P¹(30), P²⁴(55) and P¹(55) adsorbent materials was carried out in 100 mL polypropylene flasks, by adding 0.1 g of adsorbent in 50 mL of Pb(II) aqueous solution with initial concentration of 100 and 1500 mg/L, respectively. The pH of the initial solution was adjusted to

5.0 to prevent Pb(II) ion precipitation. The flasks were shaken on a mechanical shaker at a speed of 300 rpm for 2 h, at a temperature of 25 ± 2 °C. The concentration of Pb(II) was determined after sample filtration through a 0.45 μm nitrocellulose membrane and dilution, by FAAS. Prior to the metal ion adsorption studies, the kinetic studies were performed under the same conditions, for three different concentrations of lead (100, 500 and 1000 mg/L) at different times in the range of 5–120 min in order to study the influence of adsorption time on equilibrium sorption capacity (q_e).

The removal percentage $R\%$ (Equation (1)) and the quantity of lead adsorbed q_e (Equation (2)) were calculated using the following equation:

$$R\% = \frac{C_0 - C_t}{C_0} \times 100 \quad (1)$$

$$q_e = \frac{V(C_0 - C_e)}{m}, \quad (2)$$

where: q_e is the equilibrium sorption capacity measured in $\text{mg}\cdot\text{g}^{-1}$, V is the volume of the aqueous phase in L, m is the quantity of sorbent expressed in g, and C_0 , C_t and C_e are the initial and residual concentration of the metal ion in the aqueous phase at time t , and the concentration at equilibrium, respectively ($\text{mg}\cdot\text{L}^{-1}$).

The effect of the solution pH was studied for all samples under the same conditions. A 200 $\text{mg}\cdot\text{L}^{-1}$ Pb(II) solution with initial pH values in the range 2–6, and temperature of 25 ± 2 °C was used. The experiments were performed in polypropylene flasks containing 10 mL of Pb(II) solution of each pH value and 0.02 g of sample. After stirring for 2 h, and subsequent filtration and dilution, the lead concentration in the solution was determined by FAAS. At the end of the sorption experiments, the solution pH was measured and compared to that of the initial solution.

3. Results and discussions

3.1. Characterization of LDH-based materials

All samples were structurally and texturally characterized before and after Pb(II) adsorption. In the last case, the samples were dried at 80 °C under vacuum prior the analysis.

The selected SEM images of the investigated samples (Figure 1) revealed their specific morphology, ranging from flower-like microspheres, branching

from the center in all directions, to agglomerated structures in the form of distinct platelets. After adsorption, an increase in particle agglomeration was evident.

The elemental analysis of the samples from the EDX spectra (Table 1) indicated that P²⁴(30) and P²⁴(55) materials adsorbed the largest quantity of lead on their surface. When the MgAl-LDHs samples were immersed into the Pb(NO₃)₂ acidic solution, a part of Mg²⁺, HO⁻ and CO₃²⁻ have dissolved into the solution. The dissolved HO⁻ and CO₃²⁻ anions caused the precipitation of Pb²⁺ as Pb(OH)₂(CO₃)₂ on the surface of the LDHs. The same behavior was reported for similar MgAl-LDHs obtained by different methods [24–26]. A correlation between the adsorbed lead on the one hand and synthesis temperature and ageing time on the other can be established. Thus, the ratio between adsorbed lead and lattice aluminum strongly increase with increasing temperature and ageing time. The concentration in atomic percentages of Mg generally decreased after the ionic sorption of Pb(II), with P¹(30), P²⁴(55) and P¹(55) samples exhibiting the largest decrease. As the Mg/Al atomic ratio did not change significantly before and after the retention of Pb(II) ions for all the samples except P¹(55), we can presume that the analyzed samples kept their LDHs' characteristic lamellar structure (also confirmed by from XRD analysis), and the Mg²⁺ ions on the surface were leached in the acidic solutions used for the adsorption studies. Furthermore, the concentration of Mg²⁺ was determined by ICP-OES being around 8.9 mg/L for all samples, suggesting the partial dissolution of the hydroxyl layers of the hydrotalcites.

From the EDX analysis (Table 1) it was found that the observed Mg/Al ratios of the different analyzed samples did not correspond to the theoretical value (Mg/Al = 2). According to the results previously published [27], this is due to the pH fluctuations during the LDH synthesis. The minimization of the pH influence on Mg/Al ratio during LDH synthesis will be addressed in a future study.

The FTIR spectra of P¹(30) and P²⁴(30) samples are shown in Figure 2. Both spectra present broad maxima in the range 3700–3200 cm^{-1} ascribed to several contributions: the stretching vibrations of OH groups of the LDH layers and of water molecules between the brucite layers or on the material surface, CO₃²⁻-H₂O bridging and H-bonded modes [28].

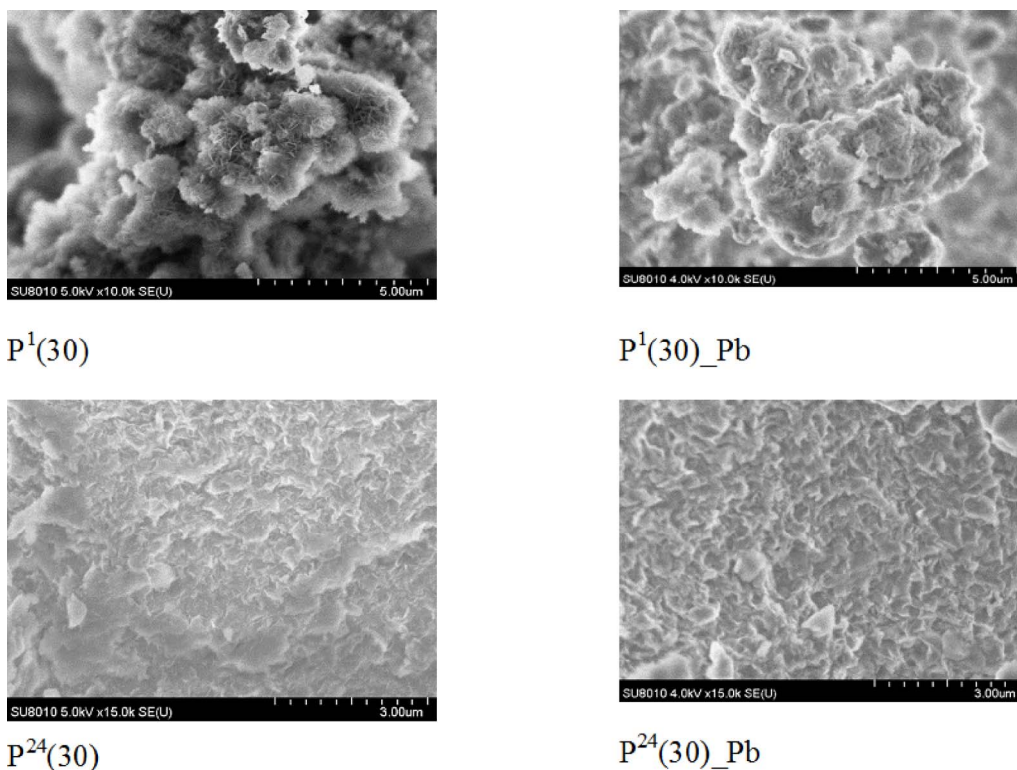


Figure 1. SEM images of LDH before and after metallic ion adsorption.

Table 1. EDX analysis results of MgAl–LDH materials before and after Pb(II) adsorption

Atomic ratio	P ²⁴ (5)		P ²⁴ (15)		P ²⁴ (30)		P ¹ (30)		P ²⁴ (55)		P ¹ (55)	
	Before	After	Before	After	Before	After	Before	After	Before	After	Before	After
Mg/Al	2.00	1.93	1.51	1.65	2.20	2.33	2.71	2.71	2.40	2.49	2.39	2.93
Pb/Al	-	0.012	-	0.049	-	0.518	-	0.036	-	0.579	-	0.121

In the case of P¹(30) sample, the maximum of this peak appears around 3490 cm⁻¹ and may be assigned to the O–H stretching in the bicarbonates species partially substituting for surface hydroxyls [29]. The peak located at 1390–1360 cm⁻¹ can be attributed to the asymmetric stretching vibrations ν_3 of CO₃²⁻ anions between layers. For P²⁴(30), there is an additional peak at 1095 cm⁻¹, which can be attributed to the ν_5 stretching vibrations in interlayer and layer-anchored bicarbonate [29] or to the activation of the ν_1 adsorption band of CO₃²⁻ due to a lowering of its symmetry and to the disordered nature of the interlayer [30]. As this sample was matured for 24 h

in air, it is possible that the atmospheric CO₂ was absorbed and anchored as bicarbonate/carbonate anions in the interlamellar region during this longer ageing period compared to 1 h for P¹(30). In the last case, the CO₂ adsorption occurs preferentially on the LDH's surface.

The peaks located in the range 770–600 cm⁻¹ correspond to the lattice vibrations of the M–O, O–M–O, M–O–M bonds (M = Mg and Al) [31]. The intensity of the peaks in the 3500–3300 cm⁻¹ region and in the carbonate/bicarbonate region increased after Pb(II) adsorption, indicating the formation of a higher quantity of Pb(OH)₂, PbCO₃ or Pb₃(CO₃)₂(OH)₂

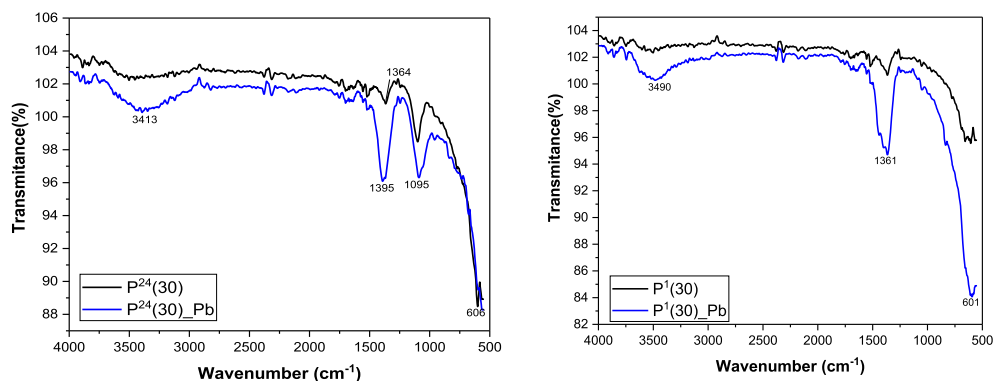


Figure 2. FTIR spectra of MgAl-LDHs obtained at 30 °C with different ageing times, before and after Pb(II) adsorption.

during the adsorption process on the surface of LDH layers (Pb-LDH).

Figure 3 shows the XRD patterns of all MgAl-LDH samples before and after Pb(II) adsorption. All samples presented the characteristic peaks of LDH structure [32,33], this being highlighted by the presence of high intensity peaks of the diffraction planes (003) ($2\theta = 11.2^\circ$), (006) ($2\theta = 22.8^\circ$), (009) ($2\theta = 34.5^\circ$) and 2 peaks of low intensity corresponding to planes (110) and (113) ($2\theta = 60\text{--}62^\circ$) [8]. The observed reflections can be indexed as the three-layer **3R** polytype with rhombohedral symmetry (space group $R\bar{3}m$).

The basal spacing corresponding to the first reflection (003) (Table 2) is similar to hydroxalcite-type structure with carbonate in the interlayer (7.7 Å). It corresponds to the distance between the centers of two adjacent layers. Due to the presence of the interlayer anions, the LDH basal spacing is higher than the one corresponding to brucite, with a major influence of the anion size and the hydration extent. LDH interlayer galleries contain anions and water molecules, with a complex network of hydrogen bonds between hydroxyl groups, anions, and water molecules [33]. The lowest value was obtained for the sample prepared at 5 °C, while the samples synthesized at 30 °C exhibited the highest basal spacing independent of ageing time. The low basal spacing usually indicates a more tight packing of the ions and molecules in the interlayers [34]. In this context, an increase in the ageing temperature is expected to determine an increase in basal spacing due to a more lax packing of the constituent species in the interlayers.

In numerous studies addressed to MgAl-LDHs, the reported values of a lattice parameter were in

Table 2. Structural parameters of the investigated samples

Sample	$d_{(003)}$ (Å)	$d_{(110)}$ (Å)	c (Å)	a (Å)	D (nm)
P ²⁴ (5)	7.61(9)	1.51(9)	22.8(5)	3.0(3)	4.5
P ²⁴ (5)_Pb	7.72(1)	1.51(2)	23.1(6)	3.0(3)	7.9
P ²⁴ (15)	8.36(9)	1.52(2)	25.1(1)	3.0(4)	5.9
P ²⁴ (15)_Pb	8.24(9)	1.52(1)	24.7(4)	3.0(4)	6.0
P ²⁴ (30)	8.36(3)	1.52(9)	25.1(1)	3.0(5)	6.1
P ²⁴ (30)_Pb	8.36(9)	1.53(2)	25.1(1)	3.0(6)	7.6
P ¹ (30)	7.81(4)	1.53(2)	23.4(4)	3.0(6)	7.1
P ¹ (30)_Pb	7.81(1)	1.52(9)	23.4(4)	3.0(6)	7.7
P ²⁴ (55)	7.81(2)	1.52(9)	23.4(4)	3.0(5)	7.9
P ²⁴ (55)_Pb	7.72(1)	1.52(7)	23.1(6)	3.0(5)	8.5
P ¹ (55)	8.03(2)	1.53(6)	24.0(9)	3.0(7)	7.7
P ¹ (55)_Pb	7.81(4)	1.53(1)	23.4(4)	3.0(6)	8.9

the range 3.02–3.07 Å, lower than the one characteristic to brucite (3.142 Å). Moreover, they decrease with the increase in Mg/Al ratio. If there is no correlation between the a value and the apparent composition of LDH, this can be an indication of the presence of other non-LDH phases. There are several factors determining the presence of broad asymmetric (01 l)/(10 l) reflections in the XRD patterns of LDH-type powders, such as low crystallite sizes and the intergrowth of rhombohedral and hexagonal polytypes [33].

After the lead adsorption experiments, the characteristic diffraction lines of the lamellar structure

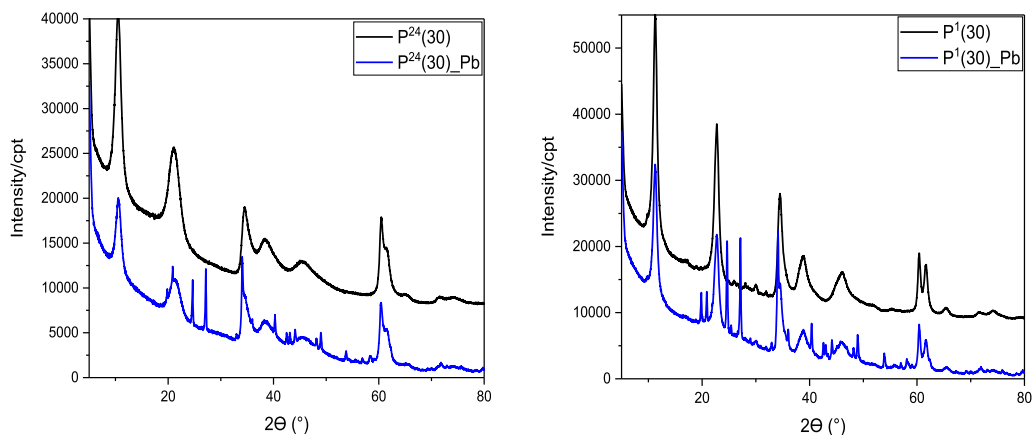


Figure 3. XRD patterns of MgAl-LDH materials obtained at 30 °C with different ageing times, before and after Pb(II) adsorption.

Table 3. Textural properties of MgAl-LDH adsorbents prepared in different synthesis conditions

Sample	BET surface area (m ² /g)	Pore volume (cm ³ /g)	Pore size (Å)
P ²⁴ (5)	9.5	0.016	57.5
P ²⁴ (15)	19.0	0.104	79.6
P ¹ (30)	25.9	0.124	87.6
P ²⁴ (30)	36.3	0.236	93.0
P ¹ (55)	57.8	0.275	124.2
P ²⁴ (55)	73.2	0.337	174.4

of the LDH decrease in intensity and additional signals appear between $2\theta = 20\text{--}27^\circ$ and $2\theta = 37\text{--}58^\circ$, which can be attributed to the corresponding crystalline phase $\text{Pb}_3(\text{CO}_3)_2(\text{OH})_2$ according to JCPDS card no. 13-0131 [35]. Also, an increase in LDH-phase crystallite size was evident, the crystallite growth being promoted by the adsorption process (Table 2).

The textural properties of the MgAl-LDH-type adsorbents were determined from N₂ adsorption-desorption isotherms at -196°C . All the investigated samples exhibited type IV isotherms with a H2 hysteresis loop, characteristic of mesoporous LDH-type powders with small amount of micropores and aggregated plate-like particles [36].

The specific surface area, pore volume and average pore size are listed in Table 3.

If we compare the S_{BET} of samples prepared at different maturation temperatures, the best results were obtained for samples synthesised at 55 °C. These samples exhibited the strongest agreement between the structural parameters (a and c from Table 2) with the characteristic ones of typical Mg/Al (2:1)-LDH [27]. All the textural parameters have increased when the maturation period increased from 1 h to 24 h, indicating an enhancement of the adsorption capacity.

3.2. Adsorption studies of Pb(II) pollutant

3.2.1. Sorption capacity of Pb(II) on MgAl-LDH adsorbents

Prior to the determination of sorption capacity of Pb(II) on MgAl-LDH adsorbents, the influence of contact time was studied for three different concentration of lead: 100, 500 and 1000 mg/L, respectively. According to the adsorption profile for all concentrations (data not shown) the adsorption capacity of Pb(II) has increased rapidly in the first 20 min, and reaches an equilibrium with the quantity of adsorbed lead remaining constant after 2 h. For sorption studies, two Pb(II) ions concentrations were used, namely 100 mg/L, and 1500 mg/L, in order to determine the adsorption capacity of the tested materials. Figure 4 shows the sorption capacities of Pb(II) ions on the investigated samples and the corresponding removal percentage (R%). At an initial concentration of 100 mg/L, P²⁴(55) sample absorbed

the highest quantity of metal ion (47.25 mg/g) with a removal percentage of 94.5%. There are no significant differences either between samples synthesised at different temperatures and aged for 24 h or for the samples synthesised at different temperatures and aged for 1 h. At an initial concentration of 1500 mg/L, the sample synthesised at 55 °C and aged for 24 h exhibited the highest adsorption capacity, adsorbing 1151.97 mg/g with a corresponding removal percentage of 76.96%. The results revealed that at high metal concentrations, the synthesis temperature is the most important parameter for tailoring the material adsorption capacity, as this parameter increased with the increase in the synthesis temperature, while the effect of ageing period is smaller. When we consider both the structural and textural parameters in correlation with the Pb(II) adsorption capacity it is clear that the best adsorption capacity was obtained for the adsorbent possessing a crystalline structure as similar as possible to typical MgAl-LDH material (Table 2) and the best textural parameters (Table 3).

Compared with the data from literature (Table 4), all the studied materials have similar or even higher adsorption capacities for Pb(II) ions, highlighting the potential of their use as adsorbent materials for heavy metal ions, both at low and high concentrations in the initial solution.

3.2.2. Influence of pH on Pb(II) sorption on MgAl-LDH adsorbent materials

The effect of pH on adsorption of Pb ions is shown in Figure 5. To prevent Pb(II) precipitation at high pH values, adsorption experiments were performed at pH values lower than 6. At $\text{pH} < 2$ the dissolution of the adsorbent has to be considered, which can lead to a collapse of the lamellar structure. In general, for LDH materials very low pH values are avoided in adsorption studies [49]. Also, at low pH values a protonation of the active sites of the adsorbent takes place and thus an electrostatic repulsion occurs between these positive charged active sites and the positive metal ions, also positive.

It was observed that the removal ratio of Pb(II) ions generally increases with pH, all materials exhibiting a maximum efficiency at a pH value of 5. P²⁴(5) and P²⁴(15) samples showed a decreased adsorption capacity when pH ranges between 2 and 4, followed by an increase in the maximum adsorption at pH = 5 and a subsequent decrease at pH = 6. The

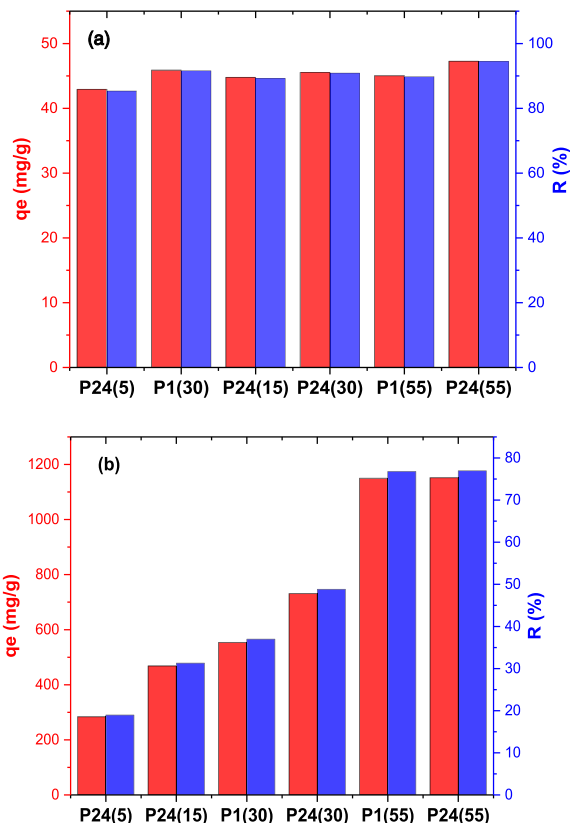


Figure 4. Adsorption capacity and the corresponding removal ratio ($R\%$) for MgAl-LDH samples at (a) $C_i = 100$ mg/L and (b) $C_i = 1500$ mg/L.

smaller adsorption capacity of lead in the pH range of 2–4, is probably due to a smaller quantity of hard-to-reach carbonate anions in their interlayer region, as the maturation temperature was not enough for carbonate retention in the interlamellar space. The same samples presented a higher adsorption capacity at $\text{pH} = 2$, due to an accelerated Mg leaching which favored the interlayer anions release. For P²⁴(30), P¹(30), P²⁴(55) and P¹(55) samples, an increase in Pb(II) adsorption was observed in the pH range 2–5, followed by a slight decrease (P²⁴(30), P¹(30), P¹(55)), or a flattening (P²⁴(55)) at the pH value of 6. As the pH increases from 2 to 5, electrostatic attractive forces become stronger and the surface of the LDH becomes more accessible for sorption of metal ions. The decrease in the removal ratio of Pb(II) ions at pH values greater than 5 can be explained by transformation of Pb(II) into $\text{Pb}(\text{OH})^+$,

Table 4. Pb(II) adsorption capacity on different adsorbent materials

Material	Pb(II) adsorption capacity (mg/g)	Ref.
FeMnMg-LDH	421.42	[13]
Chitosan/MgAl-LDH nanocomposite	333	[34]
ZnFe-LDH intercalated with citrate ions	94.3	[8]
Fe ₃ O ₄ /GO/MgAl-LDH	173	[37]
Polysulphide/MgAl-LDH	483	[38]
Sulfonated lignin/MgAl-LDH	123	[39]
MnO ₂ /MgAl	49.87	[40]
Glutamate/MgAl	68.49	[41]
MoS ₄ ²⁻ /MgAl-LDH	290	[42]
Mg ₂ Al-LDH	66.16	[19]
MgFe-LDH	865.36	[20]
MgAl-phenylalanine-LDH	852	[21]
MgAl/LDH/carbon film modified by polydopamine	1223.15	[43]
MgFeAl-CO ₃ LDH	117.86	[44]
FeMg-LDH@bentonite	1397.62	[45]
MgAl layered double oxide (LDO)	1336.80	[46]
Sludge biochar/ZnAl-LDH composite	226.10	[47]
ZnAl-LDH intercalated with amino trimethylene phosphoric acid (ATMP)	84.06	[48]
MgAl-LDH co-precipitation with different synthesis parameters	1151.97	This work

Pb(OH)₂ or Pb(OH)₃⁻; these species are stable in solution and are difficult to be adsorbed either by precipitation, complexation or electrostatic interactions. When the reaction of Pb(II) with carbonate form of Mg/Al LDH (3:1) was studied [24], an initial reaction of Pb(II) with surface hydroxide and carbonate ion was reported, with the formation of various lead precipitates. Subsequently, by decomposition of LDH structure, the interlayer carbonate could also be available for precipitation of Pb(OH)₂, Pb(CO₃)₂ and Pb₃(CO₃)₂(OH)₂. Furthermore, previous studies evidenced basic lead carbonate as the major component when the removal of Pb(II) ions from aqueous solutions was investigated using composites such as graphite-magnetite oxide-LDHs [50].

Regarding the values of the final equilibrium pH, a different tendency was noticed. Thus, for samples P²⁴(5), P²⁴(15) and P²⁴(30), the equilibrium pH values when an initial value of 2 was used, were 4.4, 4.2 and 3.4, respectively. When the initial pH is 2, the increase in final pH is probably due to the partial dissolution of the hydroxyl layers of LDHs; this behavior is also

confirmed by the presence of Mg in the final solution. An increase in the final pH for the initial pH ranging between 2 and 4 was evident, up to the maximum values of 5.1 (P²⁴(5)), 4.6 (P²⁴(15)) and 4.7 (P²⁴(30)), respectively. The pH changes could be associated with the continuous dissolution of the hydroxyl layers in order to produce the basic lead carbonate precipitation on the surface, as these pH values were not able to produce complete precipitation of Pb(II) [51]. Due to the different solubility products of lead carbonate ($K_{SP} = 1.5 \times 10^{-13}$) and lead hydroxide ($K_{SP} = 2.8 \times 10^{-16}$), the content of lead hydroxide probably exceeded that of carbonate [24]. At the initial pH of 5, where the adsorption capacity of Pb(II) was maximum, the equilibrium pH decreases to 3.6 (P²⁴(5)), 4.4 (P²⁴(15)) and 4.1 (P²⁴(30)), respectively. This behavior can be explained by the existence of a complementary mechanism of complexation of Pb(II) with the -OH groups on the surface of LDHs at this pH, with the simultaneous release of the H⁺, which is predominant over precipitation [24]. This maximum adsorption pH value is under the point of zero

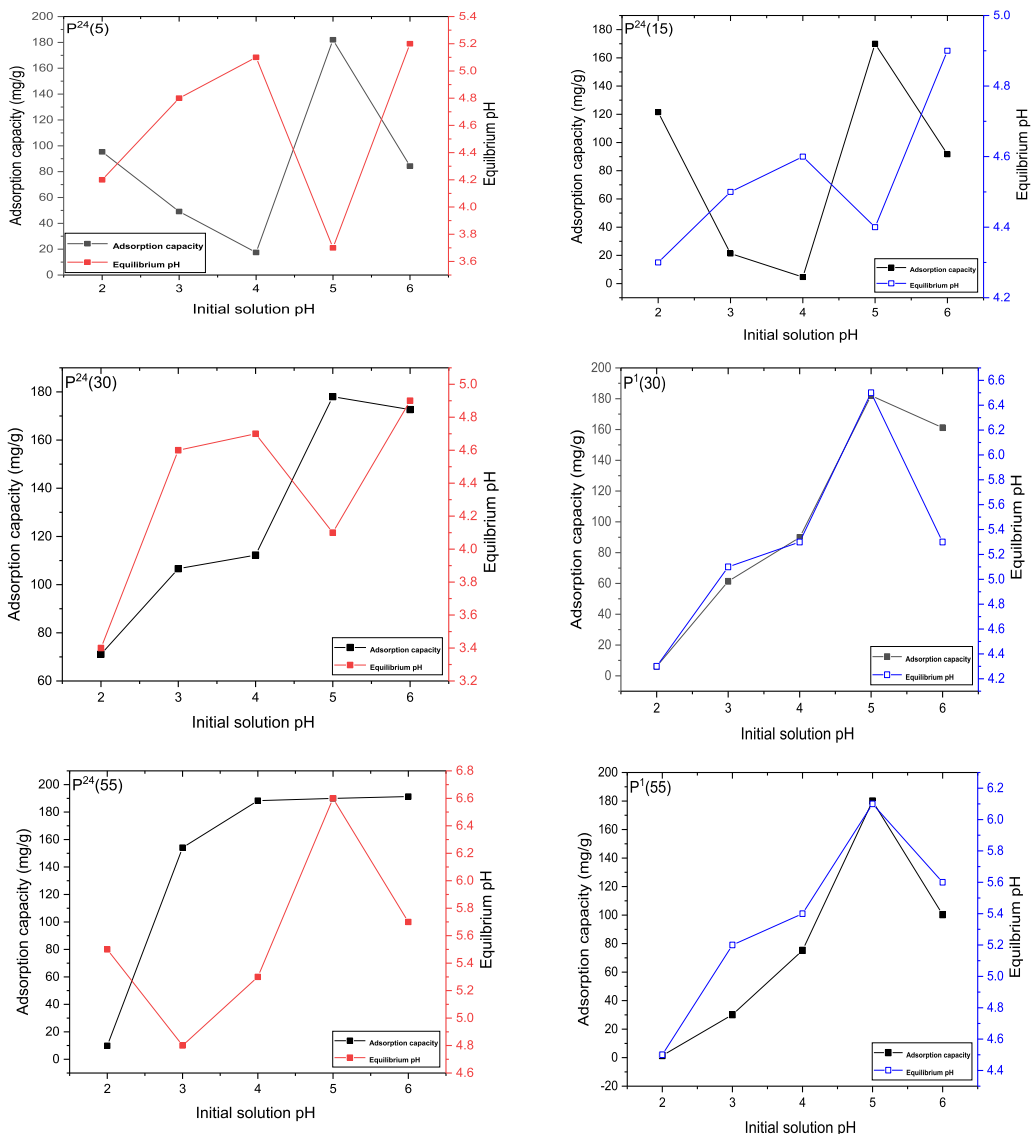


Figure 5. Effect of pH on the maximum absorption capacity of MgAl-LDH samples.

charge (pH_{pzc}) which was determined to be around 7.7 for this type of MgAl-LDHs [52]. Therefore, the surface of adsorbent is positively charged due to the protonation of surface $-OH$ groups. However, the positive charge on the surface is relatively small at this pH, as the deprotonation of LDHs increases, in comparison with more acidic $pH = 2$, allowing an increase in lead complexation by surface $-OH$ groups. For P¹(30), P²⁴(55) and P¹(55) samples, there was an increase in the equilibrium pH with respect to its initial value in the range 2–5, with the maximum values

in the range 4.4–6.6. In this case, the highest equilibrium pH values were recorded at the initial pH of 5, where the sorption capacity reaches a maximum. This behavior could be explained by a better buffering capacity of these materials compared to previous samples, due to the partial dissolution of the adsorbent and release of OH^- to increase the pH. The increase in the equilibrium pH compared to the pH of the initial solution was also noticed for other LDH materials and was ascribed to their pH buffering capacity [13]. When an LDH-Cl hydrotalcite was

used for the sorption of metal ions, the buffering capacity of the material led to a significant increase in pH [53], with precipitation of metal hydroxides being the main sorption mechanism. These hydroxides precipitated either as part of the LDH structure [51] or as separate phases [54].

For the investigated materials, it is likely that the sorption of Pb(II) ions occurs through co-precipitation mechanisms in the form of $\text{Pb}(\text{OH})_2$, PbCO_3 or $\text{Pb}_3(\text{CO}_3)_2(\text{OH})_2$ -characteristic of LDH-type materials, but also through surface complexation by bonding with the surface hydroxyl groups. Correlating the studies of the pH influence with the concentrations of Mg determined by EDX and ICP-OES analysis, we can consider that for the $\text{P}^{24}(5)$, $\text{P}^{24}(15)$, $\text{P}^{24}(30)$ samples the surface complexation by the surface hydroxyl groups has a greater influence in the global mechanism of Pb(II) ions sorption, while for the $\text{P}^1(30)$, $\text{P}^{24}(55)$ and $\text{P}^1(55)$ samples, the precipitation mechanism is predominant. The increase in Mg concentration after Pb(II) sorption is due to a partial dissolution of LDHs in order to release the corresponding anions (OH^- and CO_3^{2-}) that allow lead precipitation.

4. Conclusions

The purpose of this study was to obtain MgAl-LDH materials with improved properties toward the removal of Pb(II) ions by adjusting some of the synthesis parameters (temperature and ageing time).

The elemental analysis of the samples after adsorption indicated that $\text{P}^{24}(30)$ and $\text{P}^{24}(55)$ adsorbed the largest quantity of lead on the surface, with the preservation of their characteristic LDH lamellar structure. The stability of crystalline structure was also confirmed by XRD analysis for all the investigated samples. Moreover, XRD analysis revealed a decrease in the intensity of the characteristic peaks of the lamellar structure of the LDH after lead adsorption and the presence of additional peaks which can be attributed to the $\text{Pb}_3(\text{CO}_3)_2(\text{OH})_2$ crystalline phase.

The lead adsorption experiments have shown that at an initial concentration of 100 mg/L, sample $\text{P}^{24}(55)$ absorbs the highest quantity of metal ion (47.25 mg/g) with a removal percentage of 94.5%. At the initial concentration of 1500 mg/L, the sample absorbed 1151.97 mg/g, with a removal percentage

of 76.96%. The efficiency of Pb(II) ion removal generally increases with increasing pH value, all materials exhibiting a maximum efficiency at a pH value of 5.

Sorption of Pb(II) ions occurs through co-precipitation mechanisms in the form of $\text{Pb}(\text{OH})_2$, PbCO_3 or $\text{Pb}_3(\text{CO}_3)_2(\text{OH})_2$ characteristic to LDH materials, but also through surface complexation by bonding with the surface hydroxyl groups. By correlating the results of pH influence with the Mg concentrations determined by EDX and ICP-OES analysis we can conclude that for the $\text{P}^{24}(5)$, $\text{P}^{24}(15)$, $\text{P}^{24}(30)$ samples, the surface complexation by the surface hydroxyl groups has a greater influence in the global mechanism of Pb(II) ion sorption, while for the $\text{P}^{24}(30)$, $\text{P}^1(30)$, $\text{P}^{24}(55)$ and $\text{P}^1(55)$ samples, the increase in Mg concentration after Pb(II) sorption was due to their higher pH buffering capacity made by partial dissolution of the adsorbent and release of OH^- to increase the pH.

Further thermodynamic and kinetic studies will be performed on these materials in order to develop an efficient procedure for wastewater purification.

Conflicts of interest

Authors have no conflict of interest to declare.

References

- [1] M. Zubaira, M. Daudb, G. McKayd, F. Shehzadb, A. M. Al-Harthi, *Appl. Clay Sci.*, 2017, **143**, 279-292.
- [2] R. Verma, P. Dwivedi, *Recent Res. Sci. Technol.*, 2013, **5**, 98-99.
- [3] N. Das, R. Vimala, P. Karthika, *Indian J. Biotechnol.*, 2008, **7**, 159-169.
- [4] J. He, J. P. Chen, *Bioresour. Technol.*, 2014, **160**, 67-78.
- [5] *Guidelines for Drinking-water Quality: Fourth Edition Incorporating the First Addendum*, WHO, 2017.
- [6] P. Nagajyoti, K. Lee, T. Sreekanth, *Environ. Chem. Lett.*, 2010, **8**, 199-216.
- [7] *Inorganic and Organic Lead Compounds*, IARC Monographs on the Evaluation of Carcinogenic Risks to Humans, vol. 87, International Agency for Research on Cancer, Lyon, France, 2006.
- [8] O. Rahmanian, S. Amini, M. Dinari, *J. Mol. Liq.*, 2018, **256**, 9-15.
- [9] X. Feng, R. Long, L. Wang, C. Liu, Z. Bai, X. Liu, *Sep. Purif. Technol.*, 2022, **284**, article no. 120099.
- [10] H. Chena, J. Lina, N. Zhangb, L. Chena, S. Zhongc, Y. Wangd, W. Zhanga, Q. Linga, *J. Hazard. Mater.*, 2018, **345**, 1-9.
- [11] D. Kang, X. Yu, S. Tong, M. Ge, J. Zuo, C. Cao, W. Song, *Chem. Eng. J.*, 2013, **228**, 731-740.
- [12] K. František, G. Tomáš, D. Vít, *Solid State Sci.*, 2003, **5**, 1019-1026.

- [13] H. Zhoua, J. Zhenmao, S. Weia, *Appl. Clay Sci.*, 2018, **153**, 29-37.
- [14] C. H. Zhou, J. N. Beltramini, C. X. Lin, Z. P. Xu, G. Q. M. Lu, A. Tanksale, *Catal. Sci. Technol.*, 2011, **1**, 111-122.
- [15] L. He, Y. Huang, A. Wang, X. Wang, X. Chen, J. J. Delgado, T. Zhang, *Angew. Chem. Int. Edit.*, 2012, **51**, 6191-6194.
- [16] A. C. S. Alcantara, P. Aranda, M. Darder, E. Ruiz-Hitzky, *J. Mater. Chem.*, 2010, **20**, 9495-9504.
- [17] S. J. Ryu, H. Jung, J. M. Oh, J. K. Lee, J. H. Choy, *J. Phys. Chem. Solids*, 2010, **71**, 685-688.
- [18] U. Costantino, M. Nocchetti, M. Sisani, R. Vivani, *Z. Kristallogr.*, 2009, **224**, 273-281.
- [19] D. L. Zhao, G. D. Sheng, J. Hu, C. L. Chen, X. K. Wang, *Chem. Eng. J.*, 2011, **171**, 167-174.
- [20] X. F. Liang, W. G. Hou, J. Xu, *Chin. J. Chem.*, 2009, **27**, 1981-1988.
- [21] H. N. Trana, C. C. Linb, H. P. Chaoa, *Sep. Purif. Technol.*, 2018, **192**, 36-45.
- [22] W. Yang, W. Cai, J. Zhou, C. Dang, X. Peng, Y. Chen, X. Wei, S. Bo, S. Liang, Z. Luo, *J. Environ. Chem. Eng.*, 2021, **9**, article no. 106634.
- [23] W. T. Reichle, *Solid State Ion.*, 1986, **22**, 135-141.
- [24] M. Park, C. L. Choi, Y. J. Seo, S. K. Yeo, J. Choi, S. Komarneni, J. H. Lee, *Appl. Clay Sci.*, 2007, **37**, 143-148.
- [25] Q. Huang, Y. Chen, H. Yu, L. Yan, J. Zhang, B. Wang, B. Du, L. Xing, *Chem. Eng. J.*, 2018, **341**, 1-9.
- [26] W. Yang, W. Cai, J. Zhou, C. Dang, X. Peng, Y. Chen, X. Wei, S. Bo, S. Liang, Z. Luo, *J. Environ. Chem. Eng.*, 2021, **9**, article no. 106634.
- [27] J.-Y. Lee, G.-H. Gwak, H.-M. Kim, T. I. Kim, G. J. Lee, J.-M. Oh, *Appl. Clay Sci.*, 2016, **134**, 44-49.
- [28] K. Warmuz, D. Madej, *Appl. Clay Sci.*, 2021, **211**, article no. 106196.
- [29] J. Olszówka, R. Karcz, E. Bielańska, J. Kryściak-Czerwenka, B. D. Napruszewska, B. Sulikowski, R. P. Socha, A. Gawel, K. Bahranowski, Z. Olejniczak, E. M. Serwicka, *Appl. Clay Sci.*, 2018, **155**, 84-94.
- [30] J. T. Klopogge, D. Wharton, L. Hickey, R. L. Frost, *Am. Mineral.*, 2002, **87**, 623-629.
- [31] L. Cochechi, L. Lupa, R. Lazau, R. Voda, R. Pode, *J. Alloy Compd.*, 2019, **787**, 332-343.
- [32] J. Xu, H. Deng, J. Song, J. Zhao, L. Zhang, W. Hou, *J. Colloid Interface Sci.*, 2017, **505**, 816-823.
- [33] D. G. Evans, R. C. T. Slade, *Struct. Bond.*, 2006, **119**, 1-87.
- [34] L. Ukrainczyk, M. Chibwe, T. J. Pinnavaia, S. A. Boyd, *J. Phys. Chem.*, 1994, **98**, 2668-2676.
- [35] L. Feiyan, Y. Haiqin, H. Taille, Y. Liangguo, X. Xiaohui, D. Bin, *J. Colloid Interface Sci.*, 2019, **539**, 184-193.
- [36] S. Mohmel, I. Kurzawski, D. Uecker, D. Muller, W. Gebner, *Cryst. Res. Technol.*, 2002, **37**, 359-369.
- [37] F. Zhang, Y. Song, S. Song, R. Zhang, W. Hou, *ACS Appl. Mater. Interfaces*, 2015, **7**, 7251-7263.
- [38] S. Ma, Q. Chen, H. Li, P. Wang, S. M. Islam, Q. Gu, X. Yang, M. G. Kanatzidis, *J. Mater. Chem. A*, 2014, **2**, 10280-10289.
- [39] G. Huang, D. Wang, S. Ma, J. Chen, L. Jiang, P. Wang, *J. Colloid Interface Sci.*, 2015, **445**, 294-302.
- [40] L. Bo, Q. Li, Y. Wang, L. Gao, X. Hu, J. Yang, *J. Environ. Chem. Eng.*, 2015, **3**, 1468-1475.
- [41] S. Yanming, L. Dongbin, L. Shifeng, F. Lihui, C. Shuai, M. A. Haque, *Arab. J. Chem.*, 2017, **10**, 2295-2301.
- [42] L. Ma, Q. Wang, S. M. Islam, Y. Liu, S. Ma, M. G. Kanatzidis, *J. Am. Chem. Soc.*, 2016, **138**, 2858-2866.
- [43] W. Yang, W. Cai, J. Zhou, C. Dang, X. Peng, Y. Chen, X. Wei, S. Bo, S. Liang, Z. Luo, *J. Environ. Chem. Eng.*, 2021, **9**, article no. 106634.
- [44] A. A. Ichou, R. Benhiti, M. Abali, A. Dabagh, M. Chiban, M. Zerbet, G. Carja, F. Sinan, *Desalin. Water Treat.*, 2020, **178**, 193-202.
- [45] X. Guan, X. Yuan, Y. Zhao, J. Bai, Y. Li, Y. Cao, Y. Chen, T. Xiong, *J. Colloid Interface Sci.*, 2022, **612**, 572-583.
- [46] Y. Sun, W.-M. Yin, Y. Wang, N.-D. Zhao, X.-Y. Wang, J.-G. Zhang, Y.-R. Guo, S. Li, Q.-J. Pan, *Chem. Eng. J.*, 2022, **427**, article no. 132017.
- [47] X. Cheng, J. Deng, X. Li, X. Wei, Y. Shao, Y. Zhao, *Chemosphere*, 2022, **287**, article no. 131966.
- [48] S. Zhu, M. A. Khan, F. Wang, Z. Bano, M. Xia, *Chem. Eng. J.*, 2020, **392**, article no. 123711.
- [49] D. Tichit, O. Lorre, B. Coq, F. Prinetto, G. Ghiotti, *Microporous Mesoporous Mater.*, 2005, **80**, 213-220.
- [50] X. Liang, Y. Zang, Y. Xu, X. Tan, W. Hou, L. Wang, Y. Sun, *Colloids Surf. A*, 2013, **433**, 122-131.
- [51] M. A. González, I. Pavlovic, R. Rojas-Delgado, C. Barriga, *Chem. Eng. J.*, 2014, **254**, 605-611.
- [52] R. Benhiti, A. A. Ichou, A. Zaghoul, R. Aziam, G. Carja, M. Zerbet, F. Sinan, M. Chiban, *Environ. Sci. Pollut. Res.*, 2020, **27**, 45767-45774.
- [53] F. Zhang, Y. Song, S. Song, R. Zhang, W. Hou, *ACS Appl. Mater. Interfaces*, 2015, **7**, 7251-7263.
- [54] S. Komarneni, N. Kozai, R. Roy, *J. Mater. Chem.*, 1998, **8**, 1329-1331.